Characterization of Coplanar Waveguide Open End Capacitance—Theory and Experiment

Ming-Hua Mao, Ruey-Beei Wu, Chun-Hsiung Chen, and Chao-Hui Lin

Abstract—**The theory, numerical analysis, analytical approximate formula, measurement technique, and characteristic curves were presented in this paper for the characterization of coplanar waveguide open end capacitance. A novel variational equation was proposed in terms of the scalar potential on the slot aperture and was solved by applying the finite element method. With the available analytical Green's function and exact integration formulas in the space domain, this approach was found to be quite efficient and suitable for analyzing the coplanar waveguide discontinuity problems—even with more complicated geometrical configurations. Numerical results were compared to those obtained numerically and experimentally in previous literature, but did not correlate very well. An analytical formula under narrow-slot assumption was thus derived to render a verification of numerical results. Measurement by utilizing the resonance method were also made and the experimental data confirmed the validity of our theory. The relationship between the capacitance and the physical dimensions was also investigated. The characteristic curves of the open end capacitance were obtained. Also, an empirical formula was established for the open end structures with a thick substrate and narrow gap.**

I. Introduction

THE coplanar waveguide (CPW), first proposed in [1], offers some advantages over the conventional microstrip lines. CPW allows for easy shunt connection of passive or active components, eliminating the requirement for wraparound or via holes in the fabrication. CPW can obtain adequate propagation characteristics, e.g., small dispersion and low conductor and radiation loss up to millimeter wave frequencies under suitable design [2]. Especially, its characteristic impedance chiefly depends on the strip to slot width ratio and is relatively independent of the substrate thickness, such that the planar dimension of the circuits can be reduced while maintaining the substrate thick enough so as to sustain the structure. With the push toward high frequencies and monolithic technology in today's microwave industry, CPW has experienced a growing demand in light of the above appealing properties.

Relatively few models involving the CPW discontinuities are available even though extensive data regarding the propagation characteristics of uniform CPW can be found in previous literature [3]. Simons and Ponchak [4] presented lumped equivalent circuit models with element values deembedded from the measured scattering parameters. Frankel *et al.* determined the discontinuity capacitance or inductance from the time constant of the measured transmitted waveform under a step-like pulse excitation [5]. Naghed and Wolff applied a three-dimensional finite difference method (FDM) towards calculating the equivalent capacitance [6] and inductance [7].

Of course, the dispersion and radiation for typical CPW lines would appear as the frequencies become rather high. Alexandrou *et al.* measured the picosecond electrical pulse propagation on bent CPW structures and found that the lumped circuit models can not apply in sub-THz frequency regime [8]. The electromagnetic behavior of CPW discontinuities has recently been the focus of several investigators. By using a full-wave integral equation analysis but assuming a simple electric field distribution on the slot aperture, Drissi *et al.* calculated the scattering parameters of a radiating CPW short end [9]. Following a similar approach, Dib *et al.* considered several CPW discontinuities and derived the frequency dependent equivalent circuits [10], [11]. Nonetheless, the calculated results for the CPW short end discontinuity reveal that the end reactance varies almost linearly with frequency up to 20 GHz [9], and similarly for open end susceptance [10]. Accordingly, the end effect could be equivalently modeled by a frequency independent capacitance or inductance. This occurrence signifies that the lumped circuit models could be employed for typical CPW discontinuities at least up to the usual microwave frequency range.

Even with the above experimental or theoretical methods, more extensive and reliable data on CPW discontinuities are still required in the microwave circuit design. The CPW open end discontinuity is considered as an example, with which most of the above papers have dealt. Frankel *et al.* considered only specific structures and conveyed limited information regarding the available model [5]. Simons *et al.* presented the open end capicitance versus the gap width, but their results in [4, Fig. 6(a)] exhibited somewhat different behaviors for two quite similar structures. The FDM in [6] requires the solution of scalar potential distribution at the grid points of the three-dimensional space such that it may exhaust the available computer memory, but still have an insufficient amount of resolution to model the scalar potential in the slot region, which is of essential concern. Moreover, few of the experimental data in the above papers

Manuscript received August 31, 1992; revised August 13, 1993.

This work was supported in part by the National Science Council, Republic of China, under Grant CS 82-0210-D-002-022.

M.-H. Mao, R.-B. Wu, and C.-H. Chen are with the Department of Electrical Engineering, National Taiwan University, Taipei, Taiwan, Republic of China.

C.-H. Lin is with the Electronics Research and Service Organization, Industrial Technology Research Institute, Hsin-Chu, Taiwan, Republic of China.

IEEE Log Number 9401609.

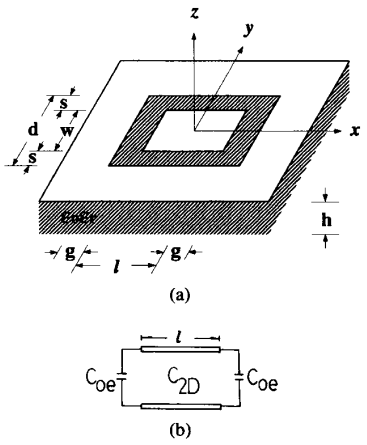

Fig. 1. (a) A three-dimensional structure for CPW open end capacitance calculation and (b) the associated equivalent circuit.

have been compared to the theoretical computation, and vice versa.

A thorough characterization of the CPW open end capacitance is therefore both theoretically as well as experimentally presented in this paper. A novel variational equation for the open end capacitance is derived in Section II in terms of the scalar potential on the two-dimensional slot aperture. In the case that the open end is of narrow gap width, the variational equation becomes simplified to an analytical formula in Section III. For more general cases, the variational equation can be solved by applying the finite element method. Section IV describes the experimental setup towards measuring the equivalent capacitance based on the resonance method. Numerical results are finally presented in Section V to provide the open end capacitance as a function of various physical dimensions and the dielectric constant of the substrate. The characteristic curves of the open end capacitance are obtained here on the basis of these results, which are quite helpful in the microwave circuit design.

II. Variational Equation for CPW Capacitance

A CPW open end structure is conventionally modeled by a section of transmission line accompanied with a lumped capacitor representing the open end capacitance C_{oe} [4]. In facilitating the capacitance analysis, two CPW open ends are connected "back-by-back" in forming a structure with a "slot loop" which is shown in Fig. 1(a). The equivalent circuit for the new structure is then illustrated in Fig. 1(b). The conductor is assumed to be of zero thickness for the sake of simplicity.

The static electric field in the source-free region is well-known to satisfy the equations

$$\nabla \cdot \epsilon \vec{E} = 0 \tag{1}$$

$$\nabla \times \vec{E} = 0. \tag{2}$$

Initiating from the curl-free nature of $\vec{E}$ in (2), the traditional approach defines a scalar potential $\phi(\vec{r})$ and finally reaches the famous variational equation in terms of electric charge [12]. Alternatively, a vector electric potential $\vec{A}_e$ can be defined from the divergence-free nature of $\epsilon\vec{E}$ in (1) such that

$$\vec{E} = -\frac{1}{\epsilon}\nabla \times \vec{A}_e. \tag{3}$$

This alternative approach is substantially more efficient than the traditional one for CPW structures, and is further exploited in this paper.

With the conductor plane as boundary, the whole space in Fig. 1(a) is divided into the upper and the lower parts. The superscript $p = u$ and l is used in the notation for denoting the quantities in the upper and lower half spaces, respectively. The total electric energy in the half space W_e^p can be found by

$$\begin{aligned} W_e^p &= \frac{1}{2}\iiint \epsilon \vec{E}^p \cdot \vec{E}^p \, d\Omega^p = -\frac{1}{2}\iiint \vec{E}^p \cdot \nabla \times \vec{A}_e \, d\Omega^p \\ &= -\frac{1}{2}\iiint [\nabla \cdot (\vec{A}_e^p \times \vec{E}^p) + \vec{A}_e^p \cdot \nabla \times \vec{E}^p] \, d\Omega^p \\ &= -\frac{1}{2}\iint_{z=0} \vec{A}_e^p \cdot \vec{E}^p \times \hat{n}^p \, dS \end{aligned} \tag{4}$$

where $\hat{n}^p$, by definition, is the unit vector outward normal to the half-space Ω^p, i.e., $\hat{n}^u = -\hat{z}$ and $\hat{n}^l = \hat{z}$. The integration in (4) requires only taking over the slots S since the tangential components of electric field vanish on the conductor. By the equivalence principle [13], the electric field would remain unchanged if the slot is filled with conductor and an equivalent magnetic current is imposed as

$$\vec{M}^p = -\vec{E}^p(z=0) \times \hat{n}^p = \nabla_t \phi(x, y) \times \hat{n}^p \tag{5}$$

where $\nabla_t = \hat{x}(\partial/\partial_x) + \hat{y}(\partial/\partial_y)$ is the gradient operator and $\phi(x, y)$ is the scalar potential on the $z = 0$ plane.

To be shown in the Appendix, the scalar Green's function G^p can be found such that

$$\vec{A}_e^p(\vec{r}) = \iint_S G^p(\vec{r}; \vec{r}\,')\vec{M}^p(\vec{r}\,') \, dS. \tag{6}$$

The capacitance between two conductors can be found from the total stored electric energy W_e in the whole space if a unit voltage drop is impressed between the two conductors. By substituting (5) and (6) into (4), the variational equation for the capacitance can be obtained in terms of the scalar potential $\phi(\vec{r})$ on the slot aperture S, i.e.,

$$\begin{aligned} C &= 2W_e = 2(W_e^u + W_e^l) \\ &= \frac{1}{2}\iint_S \iint_S G^p(\vec{r}; \vec{r}\,')\nabla_t \phi(\vec{r}) \cdot \nabla_t' \phi(\vec{r}\,') \, dS' \, dS \end{aligned} \tag{7}$$

where the Green's function $G = G^u + G^l$. The analytical formula for the Green's function in the space domain is derived in the appendix. For three-dimensional problems

$$\begin{aligned} &G(x, y, z = 0; x', y', z' = 0) \\ &\quad = \frac{\epsilon_0 + \epsilon_1}{2\pi R} + \frac{\epsilon_1}{\pi}\sum_{n=1}^{\infty}\left(-\frac{\epsilon_1 - \epsilon_0}{\epsilon_1 + \epsilon_0}\right)^n \frac{1}{\sqrt{R^2 + (2nh)^2}} \end{aligned} \tag{8}$$

where $R = \sqrt{(x-x')^2+(y-y')^2}$ and $\epsilon_1 = \epsilon_0\epsilon_r$ is the permittivity of the substrate. For two-dimensional transmission line problems

$$G(y, z=0; y', z'=0) = -\frac{\epsilon_0+\epsilon_1}{\pi}\ln\rho - \frac{2\epsilon_1}{\pi}\sum_{n=1}^{\infty}\left(-\frac{\epsilon_1-\epsilon_0}{\epsilon_1+\epsilon_0}\right)^n \ln\sqrt{\rho^2+(2nh)^2} \quad (9)$$

where $\rho = |y-y'|$.

Let $C(l)$ denote the total capacitance of the structure in Fig. 1(a). Illustrated in the equivalent circuit Fig. 1(b), $C(l)$ consists of the transmission line capacitance and the two open end capacitances. The mutual effects between the two open ends are notably assumed to be negligible in the equivalent circuit. This assumption is reasonable in common cases where the longitudinal dimensions of the line are markedly larger than its transverse dimensions. Since the transmission line capacitance is proportional to the length l, the desired open end capacitance can be obtained by

$$C_{oe} = \lim_{l\to\infty} C_{oe}(l) \quad (10)$$

where

$$C_{oe}(l) \equiv C(l) - \frac{1}{2}C(2l).$$

The mutual effects decay as the length l increases such that the extracted value $C_{oe}(l)$ tends to the exact solution C_{oe}.

III. Analytical Formula under Narrow-Slot Assumption

The magnetic current may be assumed here to flow uniformly along the slots in the case that the slots and the gap are of narrow width. Under this assumption, $\nabla_t\phi(\vec{r})$ is available and equals the given impressed voltage divided by the width. The variational equation (7) may be employed here for calculating the loop capacitance $C(l)$ and then (10) to extract the desired C_{oe}.

To evaluate the integral in (7), both the self term for which $\vec{r}$ and $\vec{r}'$ are on the same segment and the mutual term for which $\vec{r}$ and $\vec{r}'$ are on two parallel segments require consideration. The self term is in the following form and can be analytically obtained by [14]

$$\begin{aligned} f_s(s, l; \xi) &\equiv \int_0^l dx' \int_0^s dy' \int_0^l dx \int_0^s dy \cdot \frac{1}{\sqrt{(x-x')^2+(y-y')^2+\xi^2}} \\ &= \frac{4}{3}\xi^3 + \kappa(s;\xi) + \kappa(l;\xi) - 4sl\xi\tan^{-1}\frac{sl}{\xi\tau} \\ &\quad - \frac{2}{3}(l^2-2\xi^2+s^2)\tau \\ &\quad + (s^2-\xi^2)l\ln\frac{\tau+l}{\tau-l} + (l^2-\xi^2)s\ln\frac{\tau+s}{\tau-s} \end{aligned} \quad (11)$$

where the function

$$\kappa(t;\xi) \equiv \frac{2}{3}(t^2-2\xi^2)\sqrt{t^2+\xi^2} + \xi^2 t\ln\frac{\sqrt{t^2+\xi^2}+t}{\sqrt{t^2+\xi^2}-t}$$

and $\tau = \sqrt{s^2+l^2+\xi^2}$. The mutual term is in a similar form and can be expressed in terms of the above formula by [15]

$$\begin{aligned} f_m(s, l; d_s; \xi) &\equiv \int_0^l dx' \int_0^s dy' \int_0^l dx \int_{d_s}^{s+d_s} dy \cdot \frac{1}{\sqrt{(x-x')^2+(y-y')^2+\xi^2}} \\ &= \frac{1}{2s^2}[(d_s+s)^2 f_s(d_s+s, l; \xi) \\ &\quad + (d_s-s)^2 f_s(d_s-s, l; \xi) - 2d_s^2 f_s(d_s, l; \xi)] \end{aligned} \quad (12)$$

where d_s denotes the separation between the two segments. Employing the integration formulas (11) and (12), the variational equation (7) can be simplified to become

$$C(l) = \frac{\epsilon_0+\epsilon_1}{2\pi} f_{loop}(l; 0) + \frac{\epsilon_1}{\pi}\sum_{n=1}^{\infty}\left(-\frac{\epsilon_1-\epsilon_0}{\epsilon_1+\epsilon_0}\right)^n f_{loop}(l; 2nh) \quad (13)$$

where

$$f_{loop}(l;\xi) = \frac{2}{s^2}[f_s(s, l; \xi) - f_m(s, l; w+s; \xi)] + \frac{2}{g^2}[f_s(g, w+s; \xi) - f_m(g, w+s; l+g; \xi)].$$

Substituting (13) into (10) and taking the limit yields

$$\begin{aligned} C_{oe} &= \frac{1}{g^2}\left\{\frac{\epsilon_0+\epsilon_1}{2\pi} f_s(g, w+s; 0) + \frac{\epsilon_1}{\pi}\sum_{n=1}^{\infty}\left(-\frac{\epsilon_1-\epsilon_0}{\epsilon_1+\epsilon_0}\right)^n f_s(g, w+s; 2nh)\right\} \\ &\quad + \frac{1}{s^2}\left\{\frac{\epsilon_0+\epsilon_1}{2\pi} f_0(s, w; 0) + \frac{\epsilon_1}{\pi}\sum_{n=1}^{\infty}\left(-\frac{\epsilon_1-\epsilon_0}{\epsilon_1+\epsilon_0}\right)^n f_0(s, w; 2nh)\right\} \end{aligned} \quad (14)$$

where

$$\begin{aligned} f_0(s, w; \xi) &\equiv \lim_{l\to\infty}[2f_s(s, l; \xi) - 2f_m(s, l; w+s; \xi) - f_s(s, 2l; \xi) + f_m(s, 2l; w+s; \xi)] \\ &= \frac{4}{3}\xi^3 + \kappa(s;\xi) + \kappa(w+s;\xi) - \frac{1}{2}\kappa(w+2s;\xi) - \frac{1}{2}\kappa(w;\xi). \end{aligned}$$

The first part in (14) is notably the contribution from the gap, while the second part represents that due to the corner of the

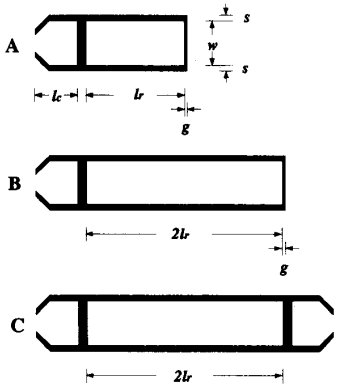

Fig. 2. Three resonators for open end capacitance measurement.

structure. For the case $\epsilon_1 = \epsilon_0$, the above expression becomes relatively simple, i.e.,

$$C_{oe}(\epsilon_r = 1) = \frac{\epsilon_0}{\pi}\left[\frac{1}{g^2} f_s(g, w+s; 0) + \frac{1}{s^2} f_0(s, w; 0)\right]$$
$$= \frac{2\epsilon_0}{\pi}\left\{(w+s)\left[\frac{\ln(\sqrt{1+\eta^2}\eta)}{\eta} + \ln\frac{\sqrt{1+\eta^2}+1}{\eta} - \frac{1}{3}\left(\frac{1}{1+\sqrt{1+\eta^2}} + \frac{1}{\eta+\sqrt{1+\eta^2}}\right)\right] - \left(w+\frac{2}{3}s\right)\right\} \quad (15)$$

where $\eta = g/(w+s)$. Although the expression in (14) is quite lengthy, the only numerical work lies in performing an infinite summation of a fast convergent geometric series.

IV. Measurement

The open end capacitance is measured here by the resonance method [16]. Three resonators are illustrated in Fig. 2. Each resonator is open-circuited at one end and is coupled with the CPW through a gap at the other. The electrical length of the resonator would be different from the physical length if taking into account the end effect. For an open end, C_{oe} is related to the length extension Δl_{oe} by

$$C_{oe} = \frac{\tan\beta\,\Delta l_{oe}}{\omega Z_0}. \quad (16)$$

Remember that $\beta = 2\pi/\lambda = 2\pi f\sqrt{\epsilon_{eff}}/c$ where f is the frequency, Z_0 is the characteristic impedance, ϵ_{eff} is the effective dielectric constant, and c is the velocity of light in free space. If $\Delta l_{oe}/\lambda$ is small, $\tan\beta\,\Delta l_{oe}$ can be approximated by $\beta\,\Delta l_{oe}$ such that C_{oe} is proportional to Δl_{oe} and can be related to the two-dimensional transmission line capacitance C_{2D} by

$$C_{oe} \cong \frac{\beta\,\Delta l_{oe}}{\omega Z_0} \cong C_{2D}\,\Delta l_{oe}. \quad (17)$$

Deriving the resonance conditions for the three resonators is not difficult, i.e.,

$$A:\ l_r + \Delta l_{cg} + \Delta l_{oe} = \frac{n_1 c}{2f_1\sqrt{\epsilon_{eff}}}$$

$$B:\ 2l_r + \Delta l_{cg} + \Delta l_{oe} = \frac{n_2 c}{2f_2\sqrt{\epsilon_{eff}}}$$

$$C:\ 2l_r + 2\,\Delta l_{cg} = \frac{n_3 c}{2f_3\sqrt{\epsilon_{eff}}} \quad (18)$$

where Δl_{cg} is the length extension which arises in light of the coupling gap and n_1, n_2, n_3 are certain integers. Choosing $n_1 = 1$, $n_2 = n_3 = 2$ and eliminating the unknown Δl_{cg} and ϵ_{eff} in (18), Δl_{oe} can be found by

$$\Delta l_{oe} = l_r\frac{1/f_1 - 1/f_3}{2/f_2 - 1/f_1}. \quad (19)$$

That is, Δl_{oe} can be completely determined by the physical length l_r and the measured resonant frequencies f_1, f_2, f_3. The desired C_{oe} is finally obtained through (17).

Three resonators with a particular gap width g are illustrated in Fig. 2 to be fabricated on the substrate in the same run. Each resonator is tapered at one end to connect a SMA female connector. The resonant frequencies are then measured by using the network analyzer HP-8510B, and from which the open end capacitance can be obtained. Unlike the de-embedding technique employed in [4], developing an equivalent circuit model for the transition section of taper and connector is not required. The experimental results should therefore be more reliable since the errors which occur as a result of the mismatch between the measured and modeled S parameters of the transition are prevented.

V. Numerical Analysis and Results

The finite element method is applied towards solving the variational equation (7) for the unknown scalar potential $\phi(x, y)$ and the capacitance C. The slot aperture is first divided into several small rectangular elements. In each element, $\phi(x, y)$ is linearly interpolated in x and y directions from the nodal values ϕ_i's at the four corners. Taking the integrals between every two elements, (7) can be expressed as

$$C = \sum_{i=1}^{N}\sum_{j=1}^{N}\phi_i G_{ij}\phi_j = \begin{bmatrix}\bar{\phi}_I \\ \bar{\phi}_B\end{bmatrix}^T\begin{bmatrix}\bar{\bar{G}}_{II} & \bar{\bar{G}}_{IB} \\ \bar{\bar{G}}_{IB}^T & \bar{\bar{G}}_{BB}\end{bmatrix}\cdot\begin{bmatrix}\bar{\phi}_I \\ \bar{\phi}_B\end{bmatrix} \quad (20)$$

where $[\bar{\bar{G}}]$ is the global matrix, an assembly of various element matrices; $[\bar{\phi}_B]$ is the vector composed of nodal values on boundaries; $[\bar{\phi}_I]$ is composed of those of the internal nodes; and the superscript T denotes the matrix transpose. The global matrix $[\bar{\bar{G}}]$ here is notably full since the integral in (7) must be taken with respect to both $\vec{r}$ and $\vec{r}'$.

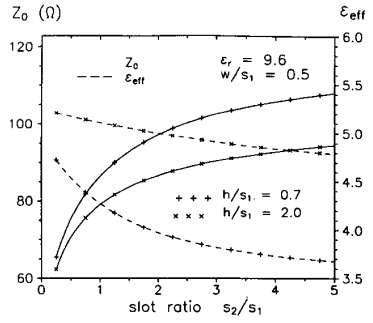

Fig. 3. Z_0 and ϵ_{eff} versus the strip width ratio s_2/s_1 for an asymmetric CPW.

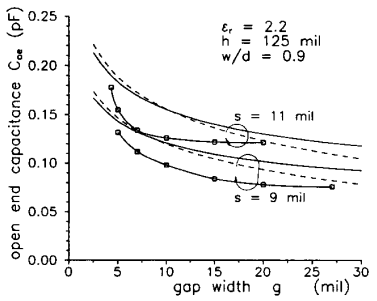

Fig. 4. C_{oe} versus the gap width g. Comparison between our numerical results (solid curves), the narrow-slot formula (dashed curves), and the experimental data which were measured over a 1 GHz band centered at 6 GHz [4] (solid curves with square marks).

Given that (20) is stationary with respect to the variation on the values of internal nodes, the following matrix equation is obtained as

$$[\bar{\bar{G}}_{II}][\bar{\phi}_I] = -[\bar{\bar{G}}_{IB}][\bar{\phi}_B]. \tag{21}$$

Note that $[\bar{\phi}_B]$ is known, when the impressed voltage is specified. The unknown potential values at the internal nodes can be solved from (21) by applying the Gaussian elimination method. The capacitance can then be obtained from (20) and can be mathematically written as

$$\begin{aligned} C &= [\bar{\phi}_B]^T\{[\bar{\bar{G}}_{IB}]^T[\bar{\phi}_I] + [\bar{\bar{G}}_{BB}][\bar{\phi}_B]\} \\ &= [\bar{\phi}_B]^T\{[\bar{\bar{H}}_{BB}] - [\bar{\bar{G}}_{IB}]^T[\bar{\bar{G}}_{II}]^{-1}[\bar{\bar{G}}_{IB}]\}[\bar{\phi}_B]. \end{aligned} \tag{22}$$

The approach is first applied toward dealing with the propagation characteristics of the CPW. The slot is divided into several small elements via numerical computation with a sinusoidal scheme [17]. Since the Green's function in (9) consists of the terms in the form $\ln|\vec{r} - \vec{r}'|$, the matrix elements in $[\bar{\bar{G}}]$ can be evaluated by employing an analytical formula derived in the Appendix of [18]. Solving the matrix equation (21) and applying (22) yields the two-dimensional transmission line capacitance C_{2D}. The characteristic impedance Z_0 and the effective dielectric constant ϵ_{eff} of the CPW can be obtained from the resultant C_{2D} in both cases that the substrate is present and absent [3]. The numerical results versus the slot ratio s_2/s_1 for an asymmetric CPW are illustrated in Fig. 3. This figure can be put into comparison with that in [19, Fig. 4]. Their consistency with each other verifies our theory in the two-dimensional case.

This approach is then next applied towards both calculating the loop capacitance $C(l)$ for the structure in Fig. 1(a) and also extracting the open end capacitance C_{oe} by (10). Exploiting the structural symmetry, the scalar potential $\phi(x, y)$ in the upper right quarter of the slot region only is required to be solved. The solution region is composed of three rectangular subregions, each of which is further subdivided in both the $x-$ and $y-$directions using the sinusoidal scheme [17].

It is very time consuming in the evaluation of the matrix element G_{ij} in (20) which is found from a quadruple integration of the Green's function in (8). In speeding up the numerical computation, the Green's function is factored into two parts: one is $(\epsilon_0 + \epsilon_1)/2\pi R$ and the other containing all those remain in (8). The first part, though simple, has a singularity at $\vec{r} = \vec{r}'$, which would be encountered in the calculation of diagonal elements. The analytical formula (11) can be employed for the integration of this part. The second part is a complicated but smooth function of the distance R. The values of the function at several discretized distances are tabulated beforehand. The function at other distances can be interpolated from the tabulated data and the quadruple integral can be calculated by Gaussian quadrature. By this way, the redundancy in calculating the Green's function is completely removed and a substantial amount of time is saved.

Let N be the smallest number of division along the $x-$ and $y-$directions of the three subregions. Several numerical examples have been executed for checking the numerical convergency by increasing the length l and the number of division N. In light of the variational nature in (7), the calculated C_{oe} decreases when either l or N increases. The convergency is satisfactory as indicated from numerical results. The deviation of C_{oe} from its limiting value would be roughly less than 1% when both l/d and N are chosen to be no smaller than 5.

A comparison of the numerical results obtained by the present method with the experimental data presented in [4] is illustrated in Fig. 4. The dashed curves are obtained by employing the narrow-slot formula (14). The numerical results are observed to be consistent with those by narrow-slot formula when the gap width g is small. When g increases, the discrepancy between them is also larger, as expected. To the contrary, the comparison between the numerical results and the experimental data in [4] is not so satisfactory. The discrepancy is quite remarkable and the experimental data are smaller than ours by 5–20%. To our knowledge, the experimental data have not been previously compared to any theoretical computations in available literature. The two structures of interest in Fig. 4 are notably the same except for a slight change in slot width s, and, consequently, the behavior of C_{oe} versus g should be similar. However, the experimental data in [4] exhibit quite inconsistent behaviors in these two cases. This inconsistency may be accounted for by the experimental errors during the de-embedding of the S parameters, which are subsequently amplified in the extraction of C_{oe} from the S parameters.

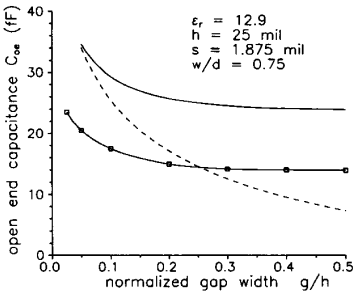

Fig. 5. C_{oe} versus the gap width g. Comparison between our numerical results (solid curve), the narrow-slot formula (dashed curve), and the results by finite difference method in [6] (solid curve with square marks).

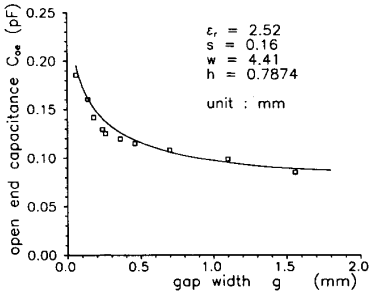

Fig. 6. C_{oe} versus the gap width g. Comparison between our numerical results (solid curve) and the experimental data obtained by the resonance technique (square marks).

In spite of this, whether the experimental errors would also cause the discrepancy between our calculated values and the experimental data still remains unclear.

A comparison of the numerical results obtained by the present method with those calculated by using three-dimensional FDM [6] is illustrated in Fig. 5. Again, the dashed curves are obtained by using the narrow-slot formula (14). The slot width s and gap width g here are not small as compared to the slot separation w. Therefore, the values by the analytical formula (14) significantly deviate from the numerical results except for when the gap width g is very small. Additionally, the numerical results are remarkably different from those by FDM, although both have an almost identical tendency versus the gap width g. The FDM results in [6], which was not supported by any results from independent sources either, are smaller than the present numerical results by roughly 40% over the whole range of gap width g.

Our numerical results apparently so far do not correlate very adequately with those in the available literature. More reliable experimental data is therefore attempted to be obtained by using the aforementioned resonance technique. A series of test structures illustrated in Fig. 2 with various gap width g have been fabricated in the substrate having $\epsilon_r = 2.52$ and a thickness of 0.7874 mm. The CPW has the dimension $w = 4.41$ mm and $s = 0.16$mm such that its characteristic impedance is 50 ohm. The length l_r is chosen to be 2.5 cm and the resonant frequencies are measured in the frequency range near 4 GHz. The experimental open end capacitances C_{oe} are

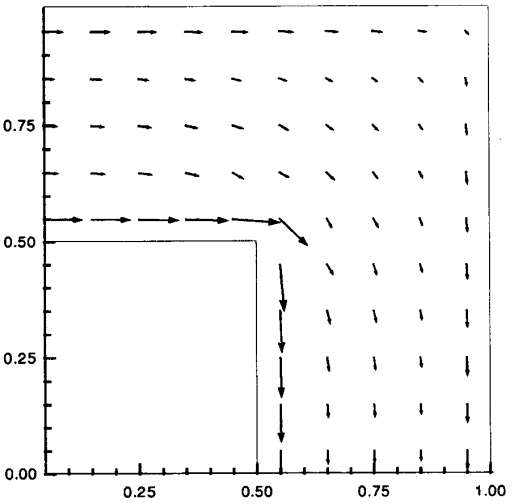

Fig. 7. A vector plot of the magnetic current in the upper right slot region of a CPW open end. The parameters are $\epsilon_r = 2.2, h = 125$ mil, $d = 160$ mil, and $w = l = d/2$.

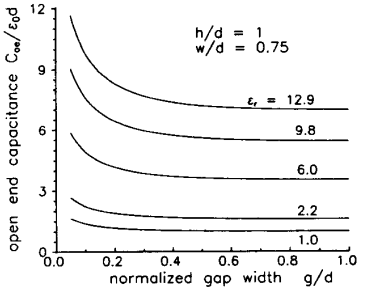

Fig. 8. Normalized open end capacitance $C_{oe}/\epsilon_0 d$ versus normalized gap width g/d with ϵ_r as a parameter.

provided in Fig. 6 and put into comparison with the numerical results. The excellent correlation between the numerical results and the experimental data markedly confirms our theory as well as our measurement technique.

A vector plot of the magnetic current around the corner is demonstrated in Fig. 7 for a typical CPW open end structure. The magnetic current distribution in the region far from the open end is observed in this figure to be longitudinal and tends to correspond with that of the uniform CPW. The magnetic current located near the corner concentrates toward the central conductor, as expected.

In characterizing the CPW open end structures, the relationship between C_{oe} and the structure parameters is finally investigated, such as the substrate thickness h, dielectric constant ϵ_r, gap width g, strip width w, and slot width s. Fig. 8 illustrates $C_{oe}/\epsilon_0 d$ versus g/d by choosing $w/d = 0.75$, $h/d = 1$, and various ϵ_r as the parameter. All of the curves indicate that C_{oe} decreases and finally saturates when the gap becomes wider. The ratio between C_{oe} and $C_{oe}(\epsilon_r = 1)$ notably maintains almost invariant versus the gap width. Furthermore, the ratio is found to be close to ϵ_{eff} with a

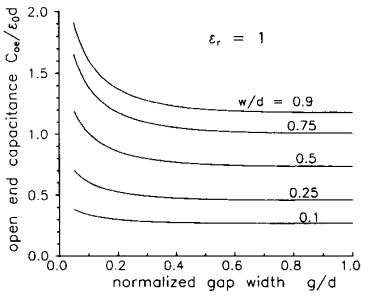

Fig. 9. Normalized open end capacitance $C_{oe}/\epsilon_0 d$ as a function of normalized gap width g/d and normalized strip width w/d in the absence of the substrate.

deviation at most 5% for each curve over the whole range of gap width. This argument remains valid at least in the common cases that $w/d \geq 0.25$ and $h/d \geq 1$, as indicated from extensive numerical studies.

Therefore, knowing the behavior of C_{oe} in the absence of the substrate is of primary interest here. The normalized open end capacitance $C_{oe}/\epsilon_0 d$ is shown in Fig. 9 as a function of the normalized gap width g/d and strip width w/d. This figure is quite helpful in characterizing the CPW open end in the microwave circuit design. In the presence of the substrate, C_{oe} can be obtained approximately by multiplying the corresponding substrate-free value with ϵ_{eff} which is dependent on w/d, ϵ_r, and h/d.

VI. Discussion and Conclusions

The CPW open end capacitance has been both theoretically and experimentally characterized successfully in this present work. A novel variational equation for the capacitance calculation is proposed and subsequently solved by applying the finite element method. Our approach is comparatively more efficient than the finite difference method in [6] since it only requires solving the potential distribution on the slot aperture rather than in the whole space. The approach can be applied towards dealing with other CPW discontinuities without a substantial amount of difficulty since the finite element method can handle more complicated shapes. Moreover, the extension of our approach from a two-dimensional transmission line problem towards a three-dimensional discontinuity problem is quite natural since the involved calculation is in the space domain. This makes our approach superior to those based on the spectral domain analysis such as [19], which becomes rather difficult in choosing a suitable global basis and taking the associated Fourier transform in a three-dimensional problem.

The numerical results have been verified from the comparison with the experimental data obtained by using the resonance technique. Extensive numerical examples are then considered for investigating the relationship between the open end capacitance and various structural parameters. The open end capacitance C_{oe} can be concluded from our numerical results to be reasonably estimated by

$$C_{oe} = \epsilon_{eff} \cdot C_{oe}(\epsilon_r = 1) \tag{23}$$

where ϵ_{eff} is available in previous literature [3] and $C_{oe}(\epsilon_r = 1)$ can be read from Fig. 9. In the case that the substrate thickness h is comparable to or larger than the transverse size d of the structure, ϵ_{eff} is approximately equal to $(\epsilon_r + 1)/2$. In the meantime, when the gap is narrow as compared to the transverse size, say $g/d \leq 0.1$, $C_{oe}(\epsilon_r)$ can be obtained from the simple analytical formula (15).

VII. Appendix
The Green's Functions

No matter for the upper or the lower half space, a layered structure, i.e., $\epsilon(\vec{r}) = \epsilon(z)$ may generally be considered here. First, it will be verified that the vector potential $\vec{A}_e^p$ due to the transverse magnetic current $\vec{M}^p$ on the ground plane can be written in the form of (6). Note that (6) also implies that $\vec{A}_e^p$ has transverse components only and is divergence-free. The former property is obvious since $\vec{M}^p$ is transverse. Given that the Green's function is in the form of $G^p(|x-x'|, |y-y'|, z; z')$ due to the transverse invariance in layered medium, the latter property can be verified since

$$\begin{aligned}\nabla \cdot \vec{A}_e^p(\vec{r}) &= \nabla_t \cdot \vec{A}_e^p(\vec{r}) \\ &= \iint_s -\nabla_t' G^p(\vec{r}; \vec{r}') \cdot \vec{M}^p(\vec{r}')\, dS' \\ &= -\oint_{\Gamma_S} G^p(\vec{r}; \vec{r}') \vec{M}^p(\vec{r}') \cdot \hat{n}_s' d\Gamma' \\ &\quad + \iint_S G^p(\vec{r}; \vec{r}') \nabla_t' \cdot \vec{M}^p(\vec{r}')\, dS' \\ &= 0. \end{aligned} \tag{A1}$$

Here, the first term in the right hand side is zero since $\vec{M}^p$ has no outward normal component along the slot boundary Γ_S, while the second term is zero since $\vec{M}^p$ is divergence-free as evident from (5).

Substituting (3) into (2) and (5) can yield the partial differential equation (PDE) and boundary condition (BC) for the vector potential. By using the aforementioned two properties of $\vec{A}_e^p$, it can be shown that the x and y components of $\vec{A}_e^p$, $(A_c, c = x, y)$, satisfy the PDE

$$-\nabla \cdot \left(\frac{1}{\epsilon} \nabla A_c\right) = 0 \tag{A2}$$

subject to an inhomogeneous Neumann BC: $(1/\epsilon(\partial/\partial n)A_c) = M_c$. The associated Green's function can therefore be conjectured to satisfy the PDE

$$-\nabla \cdot \left[\frac{1}{\epsilon} \nabla G^p(\vec{r}; \vec{r}')\right] = \delta(\vec{r} - \vec{r}') \tag{A3}$$

subject to the homogeneous Neumann BC: $\partial G^P/\partial n = 0$. To find the solution of A_c in (A2), Green's theorem

$$\begin{aligned}\iiint \left[g \nabla \cdot \left(\frac{1}{\epsilon} \nabla f\right) - f \nabla \cdot \left(\frac{1}{\epsilon} \nabla g\right)\right] d\Omega \\ = \iint \frac{1}{\epsilon} \left(g \frac{\partial f}{\partial n} - f \frac{\partial g}{\partial n}\right) dS \end{aligned} \tag{A4}$$

is applied. If $g = G^p(\vec{r}; \vec{r}')$, $f = A_c(\vec{r})$ is chosen and (A2), (A3) are employed, the Green's theorem (A4) yields the expression

$$A_c(\vec{r}') = \iint G^p(\vec{r}; \vec{r}') M_c(\vec{r})\, dS. \tag{A5}$$

Interchanging $\vec{r}$ and $\vec{r}'$ and employing the reciprocity that $G^p(\vec{r}; \vec{r}') = G^p(\vec{r}'; \vec{r})$, we finally end up with the desired expression (6).

The Green's functions G^u and G^l are next found for our original CPW structure shown in Fig. 1(a). In the upper half space there is magnetic current $\vec{M}^u$ on an infinitely large ground plane. By the image theory, the field remains unchanged in the upper half space if the ground plane is removed and $\vec{M}^u$ is replaced by 2 $\vec{M}^u$ at the same time. For the equivalent problem with source 2 $\vec{M}^u$ in free space, the vector potential is well-known to be given by

$$\vec{A}_e^u(\vec{r}) = \iint \frac{\epsilon_0}{4\pi|\vec{r} - \vec{r}'|} 2\vec{M}^u(\vec{r}')\, dS'. \tag{A6}$$

Then, by definition yields

$$G^u(x, y, z; x', y', z' = 0) = \frac{\epsilon_0}{2\pi\sqrt{(x-x')^2 + (y-y')^2 + z^2}}. \tag{A7}$$

In the lower half space, for simplicity, only the case with a layer of homogeneous substrate with permittivity ϵ_1 and height h is considered. The z axis is first reversed to make the structure "look better." By applying the two-dimensional Fourier transform, (A3) with $\vec{r}'$ at the origin becomes

$$-\frac{d}{dz}\left(\frac{1}{\epsilon}\frac{d\tilde{G}^l}{dz}\right) + \frac{1}{\epsilon}(k_x^2 + k_y^2)\tilde{G}^l = \delta(z) \tag{A8}$$

where

$$\tilde{G}^l(z; k_x, k_y) = \int_{-\infty}^{\infty}\int_{-\infty}^{\infty} G^l(\vec{r}; \vec{r}' = 0) e^{jk_x x} e^{jk_y y}\, dx\, dy.$$

The solution of the ordinary differential equation (A8) can be readily given by

$$\tilde{G}^l = \begin{cases} a\cosh uz - \frac{\epsilon_1}{u}\sinh uz & 0 \le z \le h \\ \left(a\cosh uh - \frac{\epsilon_1}{u}\sinh uh\right)e^{-u(z-h)} & z \ge h \end{cases} \tag{A9}$$

where $u = \sqrt{k_x^2 + k_y^2}$ and $a = (\epsilon_1/u)(\epsilon_0 + \epsilon_1 \tanh uh/\epsilon_0 \tanh uh + \epsilon_1)$.

It is recalled that G^l would be reduced to G^u and provided by (A7) when $\epsilon_1 = \epsilon_0$. This in turn implies the identity

$$\left.\frac{\epsilon_0}{u}e^{-uz}\right|_{u=\sqrt{k_x^2+k_y^2}} = \int_{-\infty}^{\infty}\int_{-\infty}^{\infty} \frac{\epsilon_0}{2\pi\sqrt{x^2+y^2+z^2}} e^{jk_x x} e^{jk_y y}\, dx\, dy. \tag{A10}$$

In general cases that $\epsilon_1 \neq \epsilon_0$, considered here is the Green's function on the $z = 0$ plane and expand $\tilde{G}^l$ by a Taylor expansion of e^{-uh}, i.e.,

$$\tilde{G}^l(z=0) = a = \frac{\epsilon_1}{u}\left[1 + 2\sum_{n=1}^{\infty}\left(-\frac{\epsilon_1 - \epsilon_0}{\epsilon_1 + \epsilon_0}\right)^n e^{-2nuh}\right]. \tag{A11}$$

The Green's function in the space domain can then be obtained by applying the inverse Fourier transform to (A11) and using the identity (A10). The Green's function is notably space invariant in the x and y directions. Finally, we will have

$$G^l(x, y, z=0; x', y', z'=0) = \frac{\epsilon_1}{2\pi}\left[\frac{1}{R} + 2\sum_{n=1}^{\infty}\left(-\frac{\epsilon_1 - \epsilon_0}{e_1 + \epsilon_0}\right)^n \frac{1}{\sqrt{R^2 + (2nh)^2}}\right] \tag{A12}$$

where $R = \sqrt{(x-x')^2 + (y-y')^2}$.

For the two-dimensional transmission line problem, the Green's function for the upper half space is well-known to be

$$G^u(y, z; y', z' = 0) = -\frac{\epsilon_0}{\pi}\ln\sqrt{(y-y')^2 + z^2}. \tag{A13}$$

By a similar derivation, the Green's function for the lower half space can be written as

$$G^l(y, z=0; y', z'=0) = -\frac{\epsilon_1}{\pi}\left[\ln\rho + 2\sum_{n=1}^{\infty}\left(-\frac{\epsilon_1 - \epsilon_0}{\epsilon_1 + \epsilon_0}\right)^n \ln\sqrt{\rho^2 + (2nh)^2}\right] \tag{A14}$$

where $\rho = |y - y'|$.

REFERENCES

[1] C. P. Wen, "Coplanar waveguide: A surface strip transmission line suitable for nonreciprocal gyromagnetic device applications," *IEEE Trans. Microwave Theory Tech.*, vol. MTT-17, pp. 1087–1090, Dec. 1969.

[2] R. W. Jackson, "Considerations in the use of coplanar waveguide for millimeter-wave integrated circuits," *IEEE Trans. Microwave Theory Tech.*, vol. MTT-34, pp. 1450–1456, Dec. 1986.

[3] K. C. Gupta, R. Garg, and I. J. Bahl, *Microstrip Lines and Slotlines*. Dedham, MA: Artech, 1979, Ch. 7.

[4] R. N. Simons and G. E. Ponchak, "Modeling of some coplanar waveguide discontinuities," *IEEE Trans. Microwave Theory Tech.*, vol. 36, pp. 1796–1803, Dec. 1988.

[5] M. Y. Frankel, S. Gupta, J. A. Valdmanis, and G. A. Mourou, "Picosecond pulse formation by transmission line discontinuities," *Electron. Lett.*, vol. 25, pp. 1363–1365, Sept. 1989.

[6] M. Naghed and I. Wolff, "Equivalent capacitance of coplanar waveguide discontinuities and interdigitated capacitors using a three-dimensional finite difference method," *IEEE Trans. Microwave Theory Tech.*, vol. 38, pp. 1808–1815, Dec. 1990.

[7] M. Naghed, M. Rittweger, and I. Wolff, "A new method for the calculation of the equivalent inductances of coplanar waveguide discontinuities," in *1991 IEEE MTT-S Int. Microwave Symp. Dig.*, pp. 747–750.

[8] S. Alexandrou, R. Sobolewski, H. Nakano, B. C. Tousley, and T. Y. Hsiang, "Picosecond characterization of bent coplanar waveguides," *IEEE Microwave Guided Wave Lett.*, vol. 1, pp. 236–238, Spet. 1991.

[9] M. Drissi, F. V. Hanna, and J. Citrene, "Analysis of coplanar waveguide radiating end effects using the integral equation technique," *IEEE Trans. Microwave Theory Tech.*, vol. 39, pp. 112–116, Jan. 1991.

[10] N. I. Dib and L. P. B. Katehi, "Modeling of shielded CPW discontinuities using the space domain integral equation method," *J. Electromagnetic Waves Appl.*, vol. 5, pp. 503–523, 1991.

[11] N. I. Dib, L. P. B. Katehi, G. E. Ponchak, and R. N. Simons, "Theoretical and experimental characterization of coplanar waveguide discontinuities for filer applications," *IEEE Trans. Microwave Theory Tech.*, vol. 39, pp. 873–882, May 1991.

[12] R. E. Collin, *Filed Theory of Guided Waves*. New York: McGraw-Hill, 1960, Ch. 3, 4.
[13] R. F. Harrington, *Time-Harmonic Electromagnetic Fields*. New York: Macmillan, 1961.
[14] A. E. Ruehli and P. A. Brennan, "Efficient capacitance calculations for three-dimensional multiconductor systems," *IEEE Trans. Microwave Theory Tech.*, vol. MTT-21, pp. 76–82, Feb. 1973.
[15] R. B. Wu, C. N. Kuo, and K. K. Chang, "Inductance and resistance computations for three-dimensional multiconductor interconnection structures," *IEEE Trans. Microwave Theory Tech.*, vol. 40, pp. 263–271, Feb. 1992.
[16] T. C. Edwards, *Foundation for Microstrip Circuit Design*. New York: Wiley, 1981, pp. 172–207.
[17] W. T. Weeks, "Calculation of coefficients of capacitance of multiconductor transmission lines in the presence of a dielectric interface," *IEEE Trans. Microwave Theory Tech.*, vol. MTT-18, pp. 35–43, Jan. 1970.
[18] R. B. Wu, "Resistance computations for multilayer packaging structures by applying the boundary element method," *IEEE Trans. Comp., Hygrids, Manuf. Technol.*, vol. 15, pp. 87–96, Jan. 1992.
[19] T. Kitazawa and R. Mittra, "Quasi-static characteristics of asymmetrical and coupled coplanar-type transmission lines," *IEEE Trans. Microwave Theory Tech.*, vol. MTT-33, pp. 771–778, Sept. 1985.

Ming-Hua Mao was born in Taoyuan, Taiwan, Republic of China, in 1967. He received the B.S.E.E. and M.S.E.E. degrees from National Taiwan University, Taipei, Taiwan, in 1990 and 1992, respectively.

He has been engaged in the study of propagation and discontinuity characteristics of the coplanar waveguides. Currently, he is fulfilling his duty in the military.

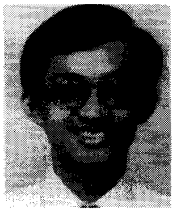

Ruey-Beei Wu was born in Tainan, Taiwan, Republic of China, in 1957. He received the B.S.E.E. and Ph.D. degrees from National Taiwan University, Taipei, Taiwan, in 1979 and 1985, respectively.

In 1982, he joined the faculty of the Department of Electrical Engineering, National Taiwan University, where he is now a Professor. From March 1986 to February 1987, he was a Visiting Scientist in IBM General Technology Division laboratory, East Fishkill Facility, Hopewell Junction, NY. His areas of interest include computational electromagnetics, dielectric waveguides, slot antennas, transmission line discontinuities, and interconnection modeling for computer packaging.

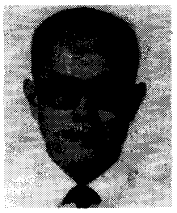

Chun Hsiung Chen was born in Taipei, Taiwan, Republic of China, on March 7, 1937. He received the B.S.E.E. degree from National Taiwan University, Taipei, Taiwan in 1960, the M.S.E.E. degree from National Chiao Tung University, Hsinchu, Taiwan, in 1962, and the Ph.D. degree in electrical engineering from National Taiwan University in 1972.

In 1963, he joined the faculty of the Department of Electrical Engineering, National Taiwan University, where he is now a Professor. From August 1982 to July 1985 he was Chairman of the department. In 1974 he was a Visiting Researcher for one year in the Department of Electrical Engineering and Computer Sciences, University of California, Berkeley. From August 1986 to July 1987, he was a Visiting Professor in the Department of Electrical Engineering, University of Houston, Houston, TX. In 1989 and 1990, he visited the Microwave Department, Technical University of Munich, Germany, and Laboratoire d'Optique Electromagnetique Faculte des Sciences et Techniques de Saint-Jerome, Universite d'Aix-Marseille III, France, respectively. His areas of interest include antenna and waveguide analysis, propagation and scattering of waves, and numerical techniques in electromagnetics.

Chao-Hui Lin was born in Taichung, Taiwan, Republic of China, in 1966. He received the M.S.E.E. degree from National Taiwan University, Taipei, Taiwan, in 1990.

He worked on microwave imaging during his graduate study. Currently, he is engaged in the design of MMIC's and microwave package, and holds several patents in this field.